CONFIDENTIAL

Copy
RM L54D15

NACA RM L54D15

RESEARCH MEMORANDUM

EXPERIMENTAL EVIDENCE OF SUSTAINED COUPLED LONGITUDINAL AND LATERAL OSCILLATIONS FROM A ROCKET-PROPELLED MODEL OF A 35° SWEPT WING AIRPLANE CONFIGURATION

By James H. Parks

Langley Aeronautical Laboratory
Langley Field, Va.

CLASSIFICATION CHANGED

To UNCLASSIFIED

By authority of Naca Res abs. Effective
LRN-114 Date 4-8-57
NB 4-30-57

CLASSIFIED DOCUMENT

This material contains information affecting the National Defense of the United States within the meaning of the espionage laws, Title 18, U.S.C., Secs. 793 and 794, the transmission or revelation of which in any manner to an unauthorized person is prohibited by law.

NATIONAL ADVISORY COMMITTEE
FOR AERONAUTICS

WASHINGTON

May 28, 1954

CONFIDENTIAL

 [redacted]

NATIONAL ADVISORY COMMITTEE FOR AERONAUTICS

RESEARCH MEMORANDUM

EXPERIMENTAL EVIDENCE OF SUSTAINED COUPLED LONGITUDINAL AND LATERAL OSCILLATIONS FROM A ROCKET-PROPELLED MODEL OF A 35° SWEPT WING AIRPLANE CONFIGURATION

By James H. Parks

SUMMARY

A rocket-propelled model of a representative 35° sweptback wing airplane design has been flight tested at high subsonic Mach numbers to investigate the possibility of the existence of coupled longitudinal and lateral motions. The model contained pulse rockets arranged to produce impulses in yaw. The flight time history is presented herein with some semiquantitative analysis.

The data indicate the existence of sustained longitudinal motions of appreciable amplitude forced by lateral oscillations. These longitudinal motions had twice the frequency of the lateral oscillations and are shown to be the result of aerodynamic moments due to sideslip and inertial cross coupling.

Feedback of the longitudinal motions into the lateral characteristics through further inertial cross coupling is shown. The roll characteristics are indicated to be the predominant influence in the inertial cross coupling.

INTRODUCTION

The concept of a pitching moment arising from a change in sideslip angle due to changes in flow conditions at the horizontal tail has been recognized for some time, and its effect is noted in reference 1. Other investigations (ref. 2, for example) have indicated the possibility of a more complex pitching moment arising from inertial coupling of yawing and rolling velocities. Recent rocket-model investigations have tended to confirm this possibility.

[redacted]

To ascertain some idea of the character and nature of these coupled longitudinal and lateral motions, the Langley Pilotless Aircraft Research Division launched a rocket model of a representative 35° swept wing airplane equipped with pulse rockets arranged to produce disturbances in yaw. This preliminary model contained only the minimum instrumentation necessary to record such motions; consequently, results are presented as experimental evidence of sustained coupled longitudinal and lateral motions with some observations and semiquantitative analysis.

SYMBOLS

M	Mach number
V	velocity, ft/sec
W	weight, lb
S	wing area, sq ft
b	wing span, ft
$\bar{c}$	mean aerodynamic chord of wing, ft
g	acceleration due to gravity, ft/sec^2
a_n	normal acceleration, ft/sec^2
a_y	lateral acceleration, ft/sec^2
a_l	longitudinal acceleration, ft/sec^2
C_N	normal-force coefficient, $\frac{W}{Sq}\frac{a_n}{g}$
C_C	chord-force coefficient, $-\frac{W}{Sq}\frac{a_l}{g}$
C_Y	side-force coefficient, $\frac{W}{Sq}\frac{a_y}{g}$
C_L	lift coefficient, $C_N \cos \alpha - C_C \sin \alpha$
C_D	drag coefficient, $C_C \cos \alpha + C_N \sin \alpha$
C_m	pitching-moment coefficient

C_n	yawing-moment coefficient
q	dynamic pressure, $0.7pM^2$, lb/sq ft
p	local static pressure, lb/sq ft
t	flight time, sec
ϵ	inclination of principal longitudinal axis with respect to the fuselage center line, deg
η	inclination of principal longitudinal axis with respect to flight path, deg
α	angle of attack, deg or radians
β	angle of sideslip, deg or radians
β_{max}	maximum angle of sideslip for particular oscillations, deg
θ	inclination of X-axis to horizontal, radians
φ	angle of bank, radians
ψ	angle of yaw, radians
γ	flight-path angle, radians
I_{X_o}	moment of inertia about principal longitudinal axis, slug-ft^2
I_{Y_o}	moment of inertia about principal lateral axis, slug-ft^2
I_{Z_o}	moment of inertia about principal vertical axis, slug-ft^2
I_X	moment of inertia about X-axis, $I_{X_o} \cos \eta + I_{Z_o} \sin \eta$, slug-ft^2
I_Y	moment of inertia about Y-axis, I_{Y_o}, slug-ft^2
I_Z	moment of inertia about Z-axis, $I_{Z_o} \cos \eta + I_{X_o} \sin \eta$, slug-ft^2
I_{XZ}	product of inertia, $-\left(I_{Z_o} - I_{X_o}\right) \sin \eta \cos \eta$, slug-ft^2

[redacted]

X	force along X-axis, lb
Y	force along Y-axis, lb
Z	force along Z-axis, lb
L	rolling moment, ft-lb
M	pitching moment, ft-lb
N	yawing moment, ft-lb
$\dot{\alpha}$, $\dot{\beta}$, $\dot{\theta}$, $\dot{\psi}$, $\dot{\varphi}$	rotational velocity; for example, $\dot{\theta} = \frac{d\theta}{dt}$, radians/sec
$\ddot{\theta}$, $\ddot{\psi}$, $\ddot{\varphi}$	rotational acceleration; for example, $\ddot{\theta} = \frac{d^2\theta}{dt^2}$, radians/sec^2

$$a = \frac{1}{2}\left(\frac{C_{L_\alpha}}{m'} - \frac{C_{m_{\dot{\alpha}}} + C_{m_{\dot{\theta}}}}{I_Y'}\right)\left(\frac{1}{57.3}\right)$$

ω	forcing frequency
ω_n	natural frequency of the model, $\sqrt{\left(-\frac{C_{m_\alpha}}{I_Y'} - \frac{C_{L_\alpha}C_{m_{\dot{\theta}}}}{m'I_Y'}\right)\left(\frac{1}{57.3}\right)}$
k	constant factor used to define a parabolic distribution of aerodynamic pitching moment with β
C_{L_α}, $C_{m_{\dot{\alpha}}}$, $C_{m_{\dot{\theta}}}$, C_{m_α}	rate of change of aerodynamic forces and moments with respect to subscripts; for example, $C_{L_\alpha} = \frac{dC_L}{d\alpha}$
m	mass of the model
m'	$\frac{mV}{qS}$
I_Y'	$\frac{I_Y}{qS\bar{c}}$
R	Reynolds numbers, based on $\bar{c}$

MODEL AND APPARATUS

A three-view drawing of the model is shown in figure 1 and the geometric and mass characteristics are tabulated in table I. Photographs of the model are shown as figure 2. Details of the construction of this type model and the basic test technique are discussed in reference 3. A discussion of the pulse-rocket technique is presented in reference 4. Locations of the pulse rockets are indicated in figure 1 and one exhaust port is evident in figure 2(a).

The model contained a six-channel telemetering installation which transmitted continuous records of normal, transverse, and longitudinal accelerations, angle of attack, angle of sideslip, and total pressure. Tracking radar and radiosonde data were used to obtain local static pressure during flight.

It is believed that the errors with this type instrumentation are primarily systematic in nature and the absolute levels are within ±0.007 in C_L, ±0.008 in C_Y, and ±0.003 in C_D at $M = 0.80$. Incremental values or slopes and variations with Mach number of the various quantities should be more accurate than the absolute values. In general, the individual instruments had natural frequencies of the order of 120 cps and damping ratios of 0.7. The accuracy of the combined α and β instrument is not completely known; however, similar vane-type instruments sensitive to angle of attack only have been shown to be accurate to about 0.3°. The Mach number is believed correct within 0.02.

The measurements made to determine the inclination of the principal longitudinal axis with respect to the fuselage center line are not considered accurate enough to determine values of less than 1°. Therefore, the value of $\epsilon = 0^\circ$ shown in table I probably is some small negative angle of less than 1°.

RESULTS AND DISCUSSION

The axis system used in this discussion is shown in figure 3. The positive directions of forces, moments, and angles are indicated in the figure. Time histories of Mach number, dynamic pressure, and Reynolds number are shown in figure 4. Angle of attack, angle of sideslip, lift coefficient, side-force coefficient, and a drag coefficient are shown in figure 5 as a function of flight time. As noted in the figures, the normal accelerometer recorded only positive values and, thus, no negative lift-coefficient values are available below approximately -0.02.

Although no measurement of the rolling velocity of accuracy comparable to that of the telemetered data was made, special radio equipment was employed to provide an order of magnitude of the rolling velocities encountered. These data are shown in figure 6. The rolling velocity of approximately ±10 radians per second with periods of the order of 0.5 second indicates that the model reached bank angles of approximately $\pm 50^{\circ}$. The order of magnitude of these bank angles was verified by the motion-picture history of the flight.

It should be emphasized here that the phase relationships between the lateral motions are quite important in the analysis of the total motion and cannot be determined from the data available with sufficient accuracy. Thus, a direct analysis of the record is virtually impossible.

The initial longitudinal disturbance (fig. 5) near $t = 3.0$ seconds is complicated by the firing of the first pulse rocket before the sustainer rocket motor burned out. At sustainer motor burnout, a longitudinal oscillation was induced by a change in trim because the thrust line was not through the model center of gravity; thus, the α and C_L values near $t = 3.0$ seconds cannot be interpreted as resulting solely from coupled motion.

The Dutch roll motion, as indicated by the sideslip oscillations, is poorly damped throughout the flight and appears dynamically unstable in the time interval $t \approx 3.6$ to $t \approx 5.0$ seconds. These trends are in general agreement with the results of reference 5 wherein dynamic lateral instability is indicated for several flight conditions. The lateral stability characteristics of similar configurations have been dealt with extensively in references 5 to 8 among others and it is beyond the scope of this report to analyze the contributing factors to these characteristics.

Aerodynamic Pitching Moment Due to Sideslip

The frequency relationship shown between α and β (period of α is one-half the period of β) is considered characteristic of the concept of coupled motions arising from changes in flow conditions of the horizontal tail since a longitudinal response to sideslip should be independent of the direction of sideslip. This effect is clearly shown by the wind-tunnel data of figure 7. Obviously, the shape of this curve will be somewhat altered at higher Mach numbers and different angles of attack; however, for the present discussion, an extrapolation of these data is not considered necessary.

The longitudinal stability data of reference 9 and the longitudinal trim data of reference 3 were used in conjunction with the data of figure 7 to approximate the angle-of-attack response by assuming $\beta = \beta_{max} \sin \omega t$ and $C_m(\beta) = k\beta^2$. When this forcing function is used in the usual two-degrees-of-freedom longitudinal equation in the form $\ddot{\alpha} + 2a\alpha + \omega_n\alpha = \frac{k\beta_{max}{}^2 \sin^2 \omega t}{I_Y{}'}$, it may be shown that the steady-state angle-of-attack response will be

$$\alpha = \alpha_{trim} + \frac{k\beta_{max}{}^2}{2I_Y{}'}\left\{\frac{1}{\omega_n{}^2} - \frac{\sin 2(\omega t + \overline{\theta})}{\left[\left(\omega_n{}^2 - 4\omega^2\right)^2 + 16a^2\omega^2\right]^{1/2}}\right\}$$

where

$$\overline{\theta} = \frac{1}{2} \tan^{-1} \frac{\left(\omega_n{}^2 - 4\omega^2\right)}{4a\omega}$$

Values of α responses computed by this method are compared with representative flight values in figure 8 at flight times where the angle-of-sideslip variation may be reasonably approximated by a sine wave. The forms of the angle-of-attack responses are quite comparable in both the computed and actual cases. While the continuous changes in altitude and Mach number introduce changes in the aerodynamic forces and moments considered as constants in the above equations (see refs. 5 and 6), these aerodynamic variations are not considered powerful enough to produce the differences shown which are most noticeable as apparent irregularities in the recorded angle of attack.

Applications of the Equations of Motion

Including Inertial Cross-Coupling Terms

It is important to note the rapid increase in α between $t \approx 3.5$ and $t \approx 4.1$ seconds (fig. 5). The incremental angle of attack is approximately doubled in two cycles of the relatively constant amplitude yawing oscillation. Also the rate of roll (fig. 6) indicates a decided increase at these flight times. Subsequent to the buildup in α, nonlinearities appear in the lateral parameters β and C_Y. Thus, it appears that the nature of the coupling is possibly dependent upon other factors in addition to the sideslip.

Further explanations for these coupled motions may be found by examination of the equations of motion for the six degrees of freedom in nonlinear form. These equations have been developed by various authors (ref. 2, for example) and may be expressed as follows:

$$mV\left[\left(\frac{\dot{V}}{V}\right) + \alpha\dot{\theta} - \beta\dot{\psi}\right] = X \tag{1}$$

$$mV(\dot{\beta} + \dot{\psi} - \alpha\dot{\phi}) = Y \tag{2}$$

$$mV(\dot{\alpha} + \beta\dot{\phi} - \dot{\theta}) = Z \tag{3}$$

$$I_X\ddot{\phi} + \left(I_Z - I_Y\right)\dot{\theta}\dot{\psi} - I_{XZ}\left(\ddot{\psi} + \dot{\phi}\dot{\theta}\right) = L \tag{4}$$

$$I_Y\ddot{\theta} + \left(I_X - I_Z\right)\dot{\phi}\dot{\psi} - I_{XZ}\left(\dot{\psi}^2 - \dot{\phi}^2\right) = M \tag{5}$$

$$I_Z\ddot{\psi} + \left(I_Y - I_X\right)\dot{\theta}\dot{\phi} - I_{XZ}\left(\ddot{\phi} - \dot{\theta}\dot{\psi}\right) = N \tag{6}$$

Note particularly the inertial terms in equations (5) and (6) which may become appreciable if I_Y and I_Z are large relative to I_X. These terms become particularly important where large roll rates are involved since $\dot{\phi}$ is a common factor in three terms and $\ddot{\phi}$ appears in the fourth. In equation (5), it is indicated that a pitching motion may be forced by a pure Dutch roll motion through inertial coupling.

These conditions are fulfilled in the present tests; that is, $I_Y \approx I_Z \gg I_X$ (table I) and high roll rates are indicated in figure 6.

Typical values of the basic rotational velocities are shown in figure 9 at flight times where these values are near maximums. These data were determined as follows: $\dot{\theta} = \dot{\alpha} + \dot{\gamma}$ where $\dot{\alpha}$ is from differentiation of angle-of-attack—time data and $\dot{\gamma} \approx \frac{C_L qS}{mV}$, $\dot{\psi}$ was computed by differentiation of angle-of-sideslip—time data and using the assumption $\dot{\psi} = -\dot{\beta}$, and the data of figure 6 were faired to obtain a continuous $\dot{\phi}$. It is readily apparent from the relative magnitude of these velocities that the roll rate is the predominant factor and should be known at least as accurately as the other data.

These velocities were used to compute the cross-coupling inertial forcing functions which are shown in figure 10. The terms $I_{XZ}\dot{\psi}^2$ and $I_{XZ}\dot{\theta}\dot{\psi}$ are omitted because $\dot{\phi}^2 \gg \dot{\psi}^2$ and $\ddot{\phi} \gg \dot{\theta}\dot{\psi}$. Included in the pitching-moment summation is the aerodynamic moment arising from sideslip as discussed previously.

For the longitudinal case, it is shown that the inertial moments are of approximately the same frequency, but of opposite sign from the aerodynamic moment due to sideslip, with the $(I_X - I_Z)\dot{\phi}\dot{\psi}$ term generally having twice the amplitude of the $I_{XZ}\dot{\phi}^2$ term. The summation of all three terms indicates an input generally having the form of $\beta_{max} \sin(2\omega t)$ similar to that indicated for the aerodynamic term alone, but of considerably greater magnitude.

For the lateral case, the inertial terms generally are of the same order of magnitude but with the $I_{XZ}\ddot{\phi}$ term effectively leading the $(I_Y - I_X)\dot{\theta}\dot{\phi}$ term. The summation of the two effects indicates a yawing moment generally having the form of $\beta_{max} \sin(3\omega t)$ and of larger amplitude than either of the contributing effects.

Harmonic Analyses of the Responses

The foregoing concepts can be further studied by harmonic analyses of the responses. The twelve ordinate scheme of harmonic analysis was used to determine the predominant frequencies contained in the angle-of-attack and angle-of-sideslip data.

The Fourier series representing the angle-of-attack data was calculated to be

$$\alpha = -1.71 - 0.30 \sin(\omega t - 85^\circ) + 2.40 \sin(2\omega t + 79.2^\circ) - 0.38 \sin(3\omega t - 64.8^\circ) + 0.13 \sin(4\omega t - 18^\circ) + 0.08 \sin(5\omega t + 45^\circ) + 0.05 \sin(6\omega t - 90^\circ)$$

This equation is represented graphically in the top plot of figure 11. Only the first three harmonics are shown, since by inspection they are of primary importance. As indicated previously, those inputs having a frequency of $2\omega t$ account almost entirely for the angle of attack. It may be of interest to note that as shown by the constant -1.71, the average effect of the various pitching moments is to induce an effective change in trim of about -1.2° since the longitudinal trim alone was determined as about -0.5° from reference 3.

The Fourier series representing the angle of sideslip was calculated to be

$$\beta = 0.12 - 7.57 \sin(\omega t + 58.2^\circ) + 0.88 \sin(2\omega t + 52.4^\circ) + 0.90 \sin(3\omega t - 48.2^\circ) + 0.12 \sin(4\omega t) + 0.08 \sin(5\omega t + 60.5^\circ) - 0.03 \sin(6\omega t + 90^\circ)$$

As in the longitudinal case, the first three harmonics are represented graphically. (See middle plot of fig. 11.) The angle-of-sideslip oscillation is composed almost entirely of the fundamental harmonic. The shape is distorted by the second and third harmonics which are approximately equal in magnitude. It would be deduced from the basic nonlinear equations that the inertial yawing moments would have the form of $\sin(3\omega t)$. The presence of an appreciable second harmonic is believed indicative of the fact that these inertial terms are not true third harmonics of the fundamental frequency.

The third harmonic is more easily identified in the side-force data. The respective Fourier series is

$$C_Y = 0.012 + 0.067 \sin(\omega t + 71.9^{\circ}) + 0.004 \sin(2\omega t + 63.5^{\circ}) + 0.016 \sin(3\omega t + 75.9^{\circ}) + 0.001 \sin(4\omega t) + 0.003 \sin(5\omega t + 90^{\circ}) + 0.001 \sin(6\omega t + 90^{\circ})$$

The first three harmonics of these data are shown in the bottom plot of figure 11 where obviously the first and third harmonics are predominant. The third harmonic represents the $\alpha\dot{\phi}$ contribution as shown in equation (2).

Response to Total Pitching Moment

Since the harmonic analysis indicates that the angle-of-attack response is primarily a second harmonic of the lateral oscillation, the response to a pitching moment having the form suggested in figure 11 and the amplitude indicated by figure 10 was computed using the two-degree-of-freedom longitudinal equations presented earlier. The results are compared with the actual response in figure 12. The agreement is considered very good considering the approximations used.

Examination of Roll Equation

It is interesting to note that the rolling velocity is probably relatively unaffected by inertial cross coupling. The term $(I_Z - I_Y)\dot{\theta}\dot{\psi}$ in equation (4) should be small because $I_Z \approx I_Y$ (table I) and both $\dot{\psi}$ and $\dot{\theta}$ are much smaller than $\dot{\phi}$. Also, in the product-of-inertia term, $(\ddot{\psi} + \dot{\phi}\dot{\theta})$ is small in comparison with $\ddot{\phi}$ or $\dot{\phi}^2$.

General Remarks

While no direct evidence is available, it is believed worth some conjecture concerning the buildup in loads. If the resonant frequency in pitch approaches twice the resonant frequency in sideslip, which was true in the present tests, it appears that prohibitive lift loads may develop rapidly during lateral maneuvers. It should be emphasized that a major portion of these loads occurs as a result of velocities and thus large amplitude displacements might be tolerated if the periods of the lateral motions are sufficiently long.

CONCLUDING REMARKS

From the flight time history of a rocket-propelled model of a representative 35° sweptback wing airplane, it is indicated that coupled longitudinal motions were excited and sustained by pure lateral oscillations. The resulting longitudinal motions had twice the frequency of the lateral oscillations and rapidly developed lift loads of appreciable magnitude.

The longitudinal moments are attributed to two sources, aerodynamic moments due to sideslip and inertial cross coupling. The roll characteristics are indicated to be the predominating influence in the inertial cross-coupling terms.

At the higher pitching rates, irregularities in the lateral data are noted. These changes are shown to be consistant with the inertial cross-coupling terms in the yawing-moment and side-force equations.

Langley Aeronautical Laboratory,
National Advisory Committee for Aeronautics,
Langley Field, Va., March 31, 1954.

REFERENCES

1. Gilruth, R. R.: Requirements for Satisfactory Flying Qualities of Airplanes. NACA Rep. 755, 1943. (Supersedes NACA ACR, Apr. 1941.)

2. Phillips, William H.: Effect of Steady Rolling on Longitudinal and Directional Stability. NACA TN 1627, 1948.

3. Parks, James H., and Mitchell, Jesse L.: Longitudinal Trim and Drag Characteristics of Rocket-Propelled Models Representing Two Airplane Configurations. NACA RM L9L22, 1950.

4. Parks, James H., and Kehlet, Alan B.: Longitudinal Stability, Trim and Drag Characteristics of a Rocket-Propelled Model of an Airplane Configuration Having a 45° Sweptback Wing and an Unswept Horizontal Tail. NACA RM L52F05, 1952.

5. Queijo, M. J., and Goodman, Alex: Calculations of the Dynamic Lateral Stability Characteristics of the Douglas D-558-II Airplane in High-Speed Flight for Various Wing Loadings and Altitudes. NACA RM L50H16a, 1950.

6. Sjoberg, Sigurd A.: Preliminary Measurements of the Dynamic Lateral Stability Characteristics of the Douglas D-558-II (BuAero No. 37974) Airplane. NACA RM L9G18, 1949.

7. Williams, W. C., and Crossfield, A. S.: Handling Qualities of High-Speed Airplanes. NACA RM L52A08, 1952.

8. Anhenbruck, Herman O., and Dahlen, Theodore E.: Some Measurements of Flying Qualities of a Douglas D-558-II Research Airplane During Flights to Supersonic Speeds. NACA RM L53A06, 1953.

9. Osborne, Robert S.: High-Speed Wind-Tunnel Investigation of the Longitudinal Stability and Control Characteristics of a 1/16-Scale Model of the D-558-2 Research Airplane at High Subsonic Mach Numbers and at a Mach Number of 1.2. NACA RM L9C04, 1949.

TABLE I

MODEL GEOMETRY AND MASS CHARACTERISTICS

Wing:	
Root airfoil section (normal to 0.30 chord)	NACA 63-010
Tip airfoil section (normal to 0.30 chord)	NACA 63_1-012
Total area, sq ft	2.97
Taper ratio	0.57
Aspect ratio	3.57
Sweepback at 0.30 chord, deg	35.0
Incidence at fuselage center line, deg	3.0
Dihedral, deg	-3.0
Geometric twist, deg	0
Horizontal tail:	
Airfoil section (normal to 0.30 chord)	NACA 63-010
Total area, sq ft	0.68
Taper ratio	0.50
Sweepback, deg	46.0
Aspect ratio	3.58
Dihedral, deg	0
Geometric twist, deg	0
Vertical tail:	
Airfoil section (normal to 0.30 chord)	NACA 63-010
Total area (to fuselage center line), sq ft	0.94
Taper ratio	0.30
Aspect ratio (based on double span)	3.57
Sweepback at 0.30 chord, deg	49
Weight, lb	56.56
Center-of-gravity location, percent $\bar{c}$	14.2
I_{X_o}, slug-ft^2	0.26
I_{Y_o}, slug-ft^2	3.21
I_{Z_o}, slug-ft^2	3.86
ϵ (referred to fuselage center line), deg	0

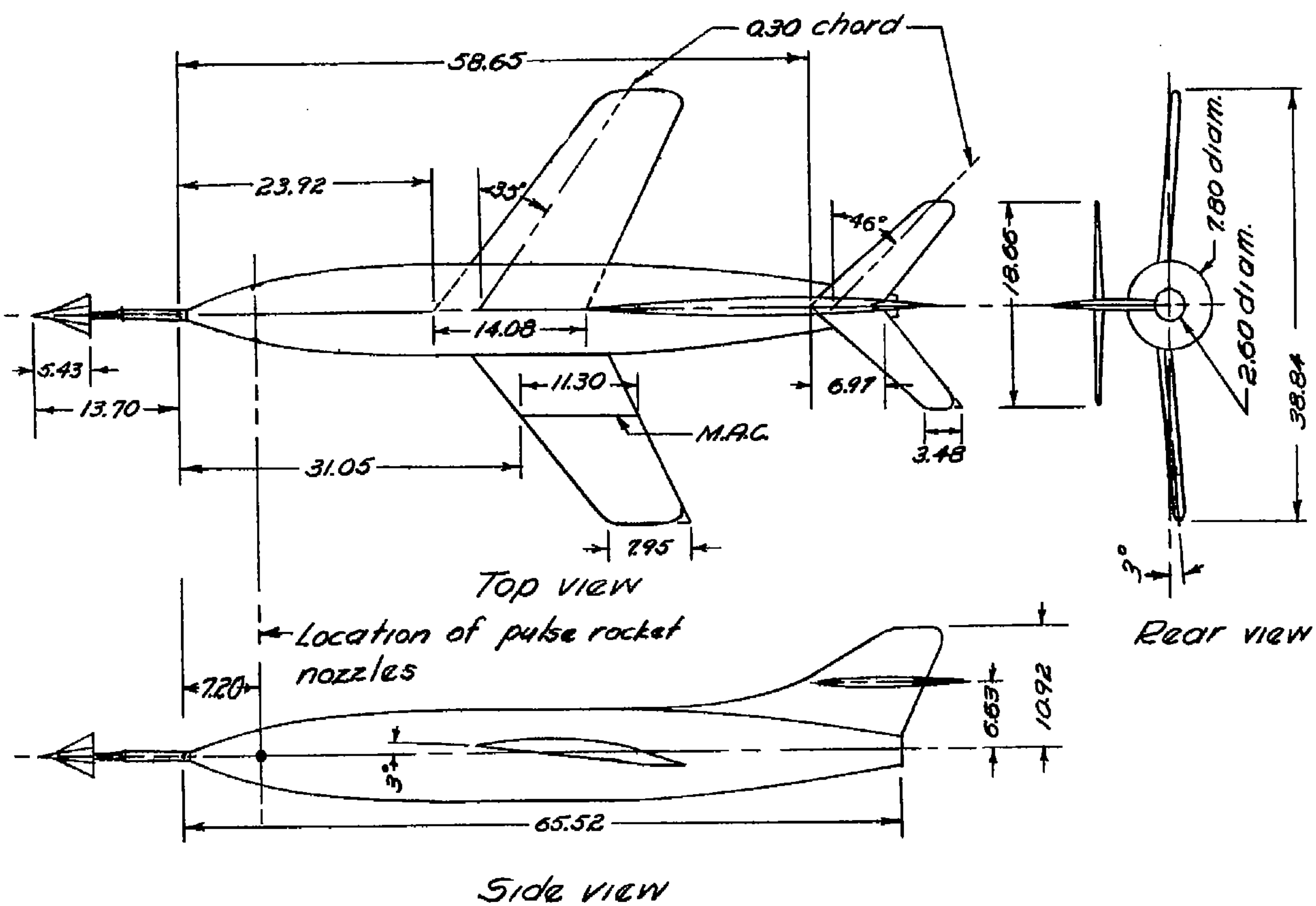

Figure 1.- General arrangement of the model. All dimensions in inches.

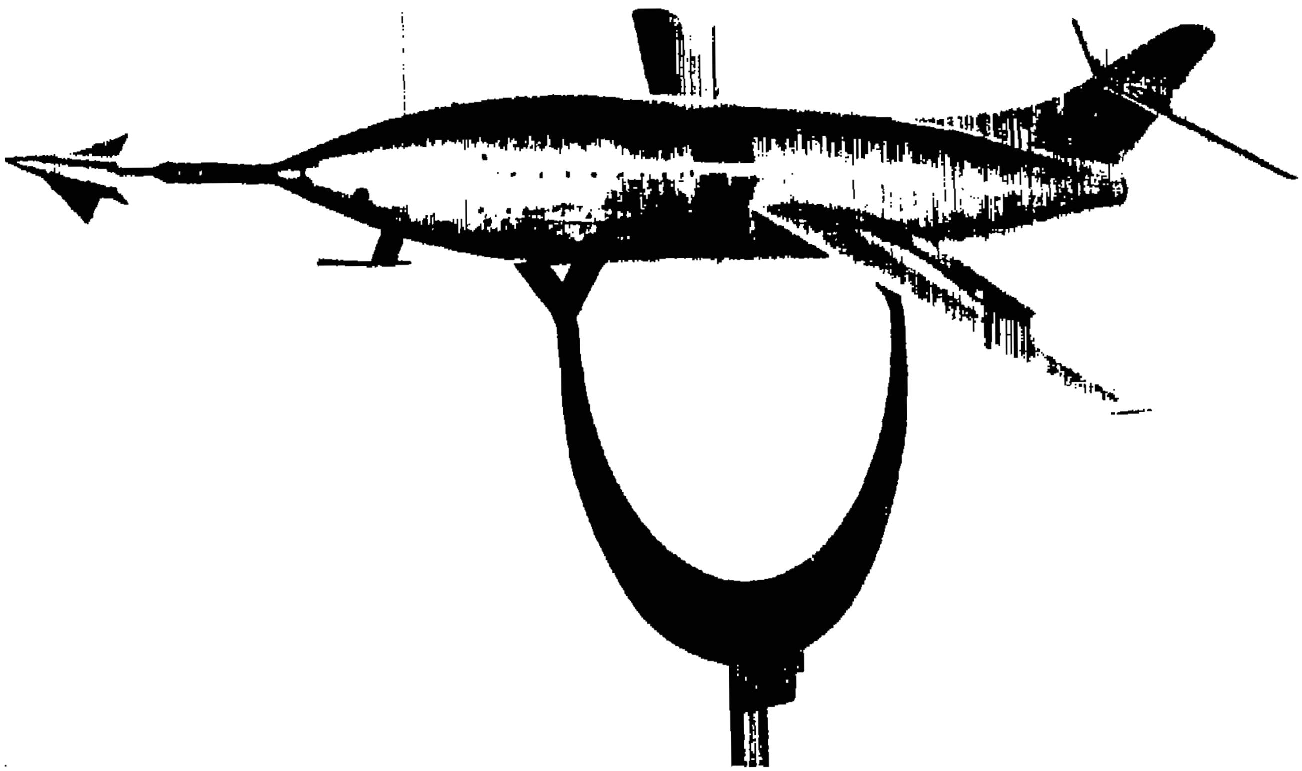

L-76420.1

(a) Model alone.

Figure 2.- Photographs of the model.

L-76554.1

(b) Model plus booster in launching position.

Figure 2.- Concluded.

F

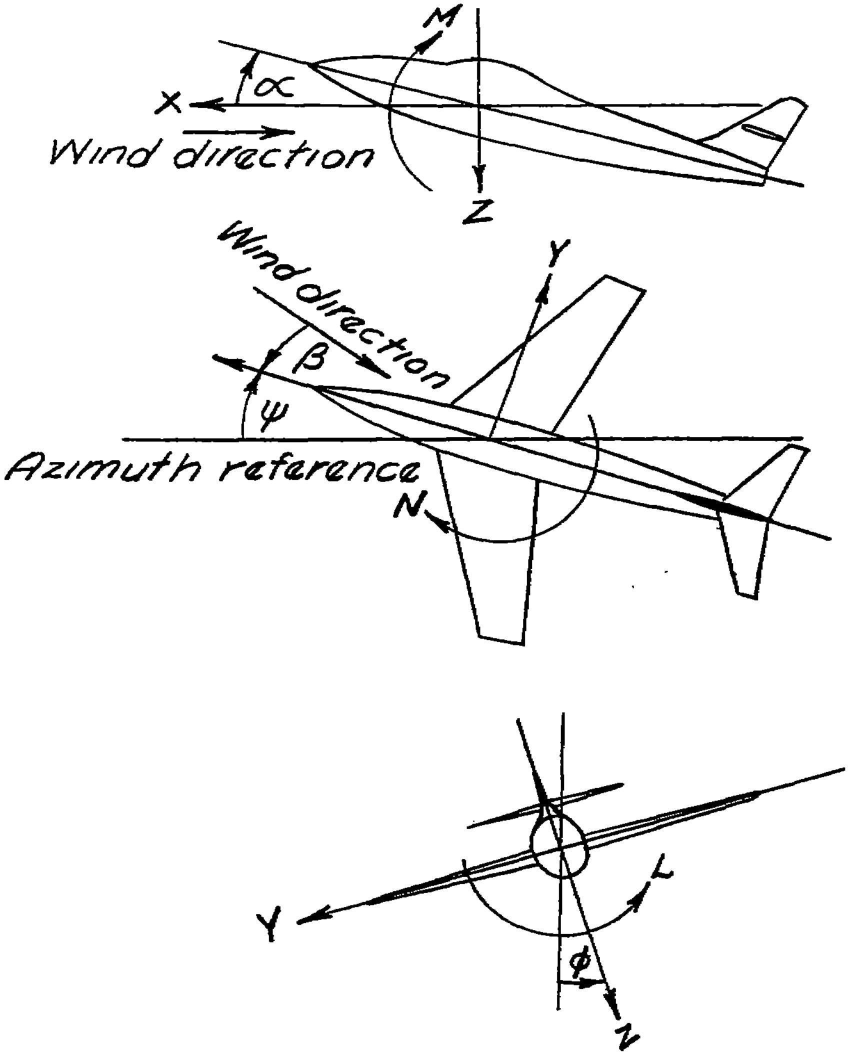

Figure 3.- The stability system of axes. Arrows indicate positive directions of moments, forces and angles. The origin is at the center of gravity.

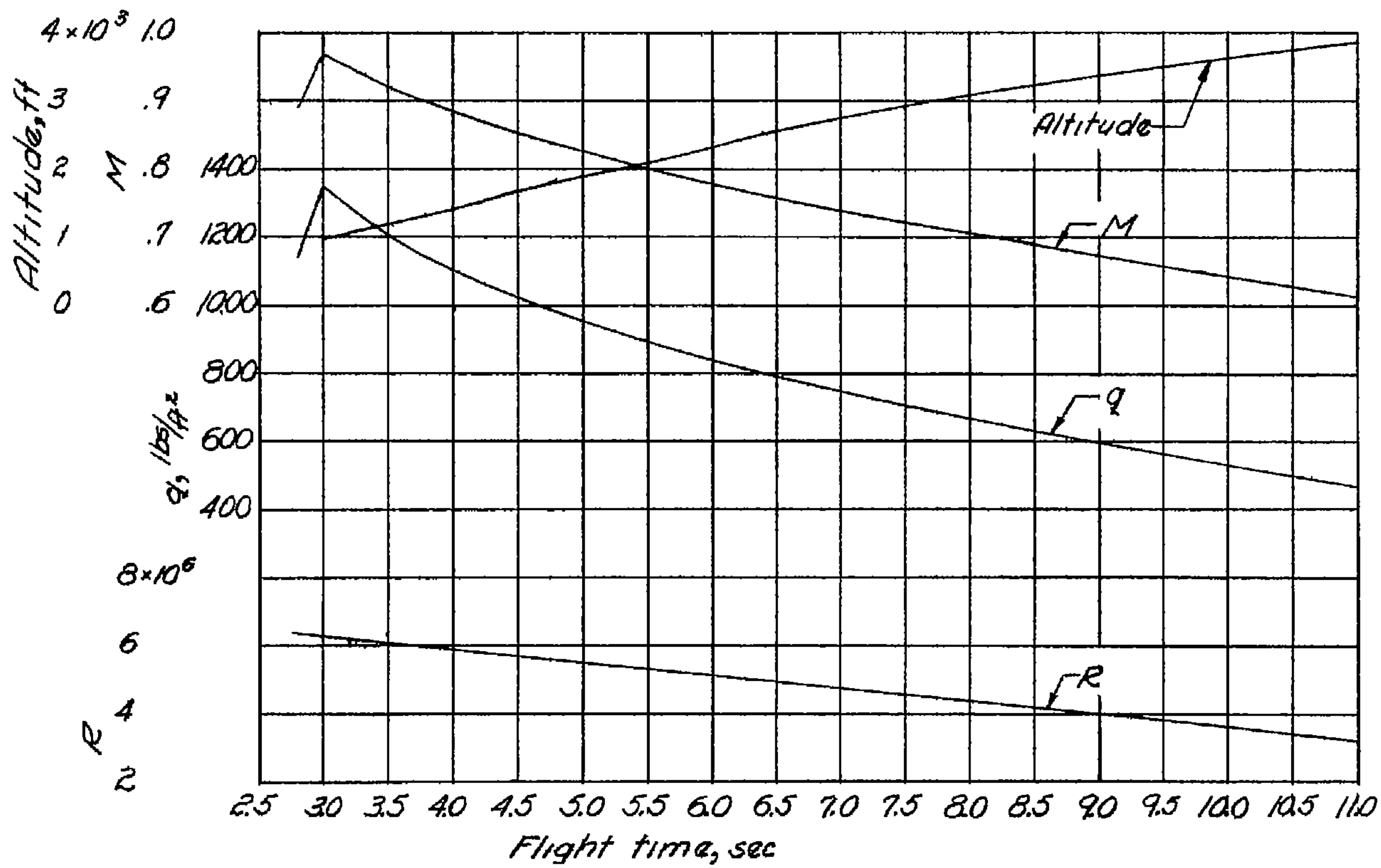

Figure 4.- Time history of altitude, Mach number, dynamic pressure, and Reynolds number.

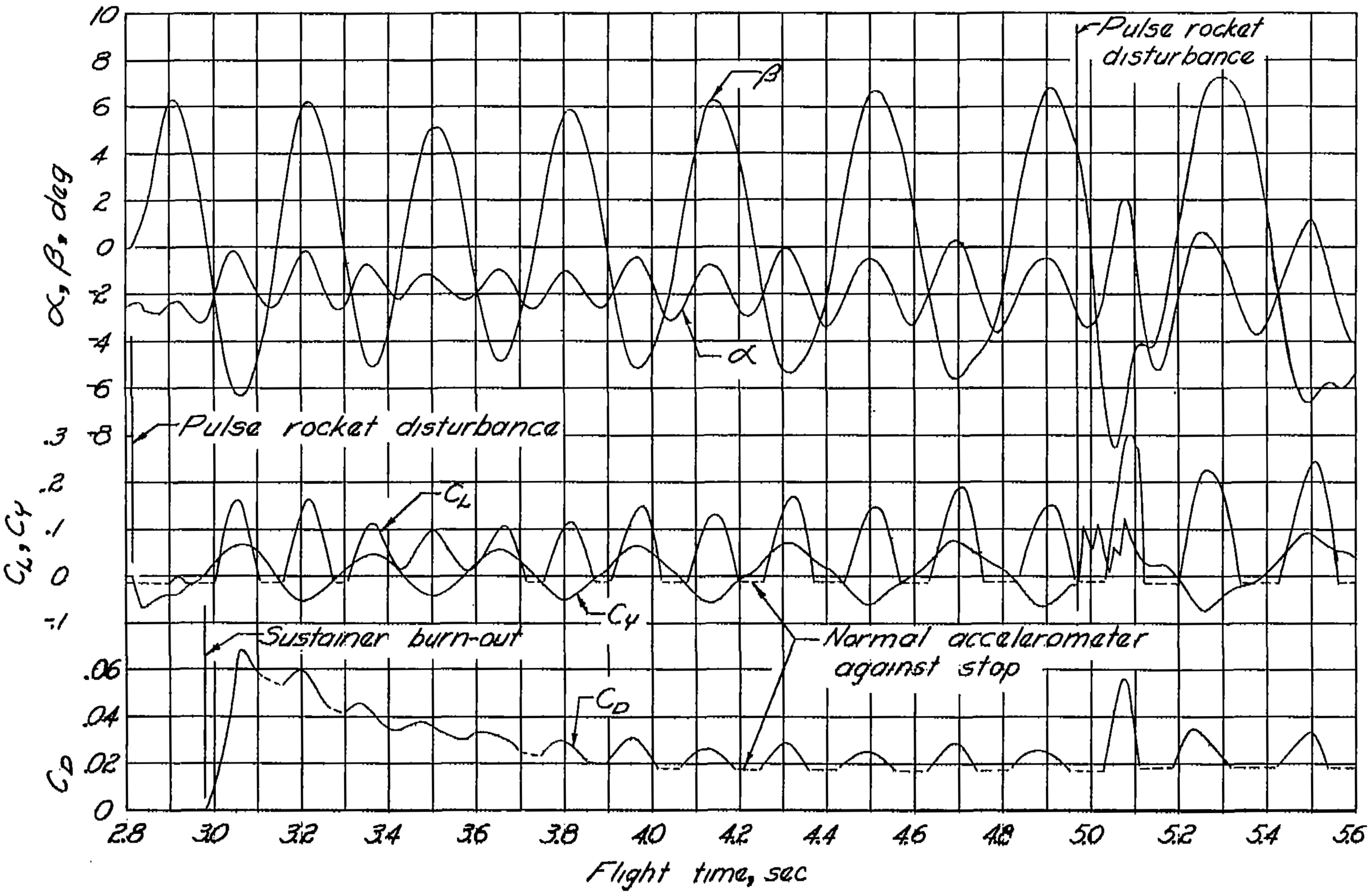

Figure 5.- Time history of the flight.

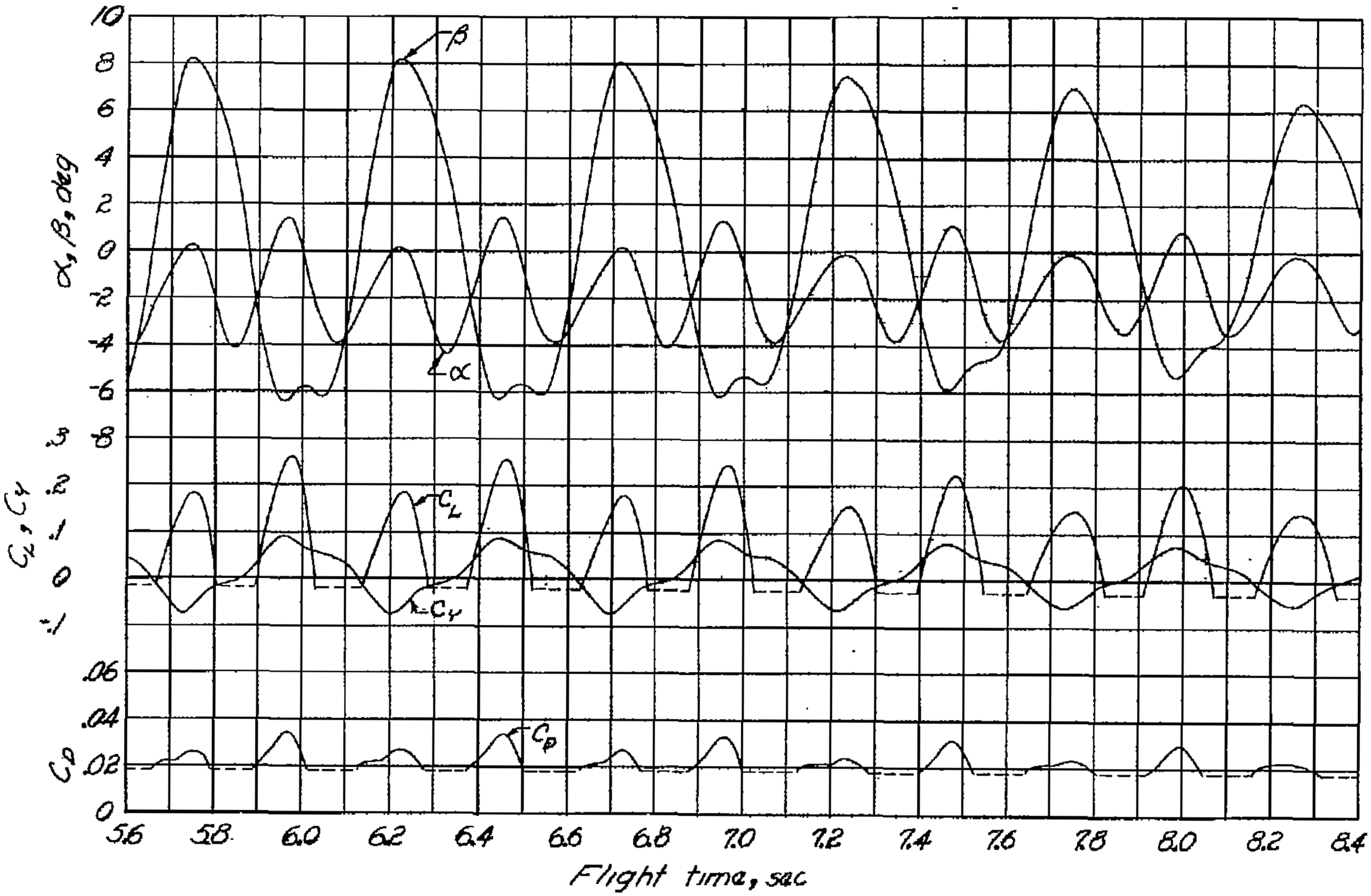

Figure 5.- Continued.

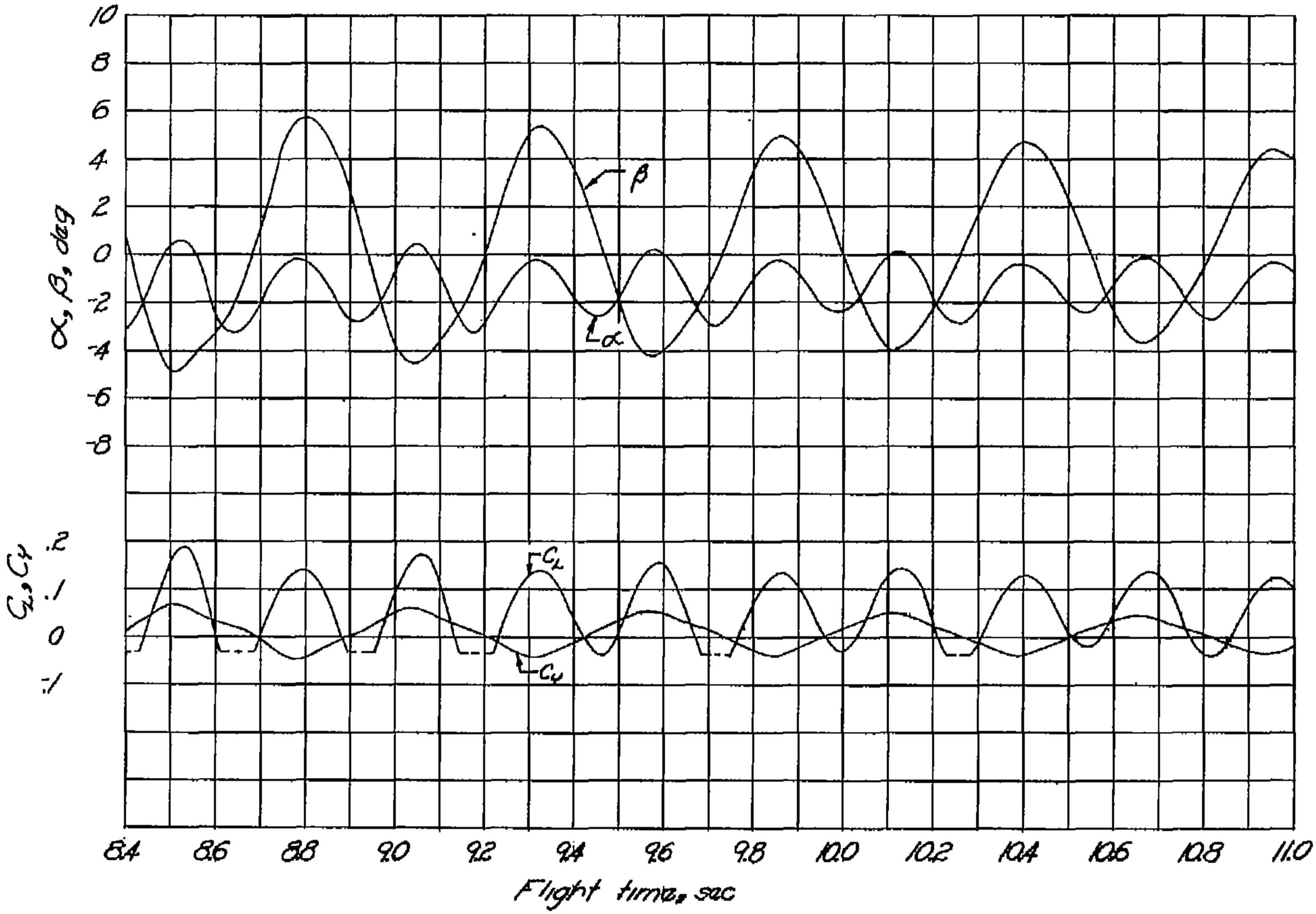

Figure 5.- Concluded.

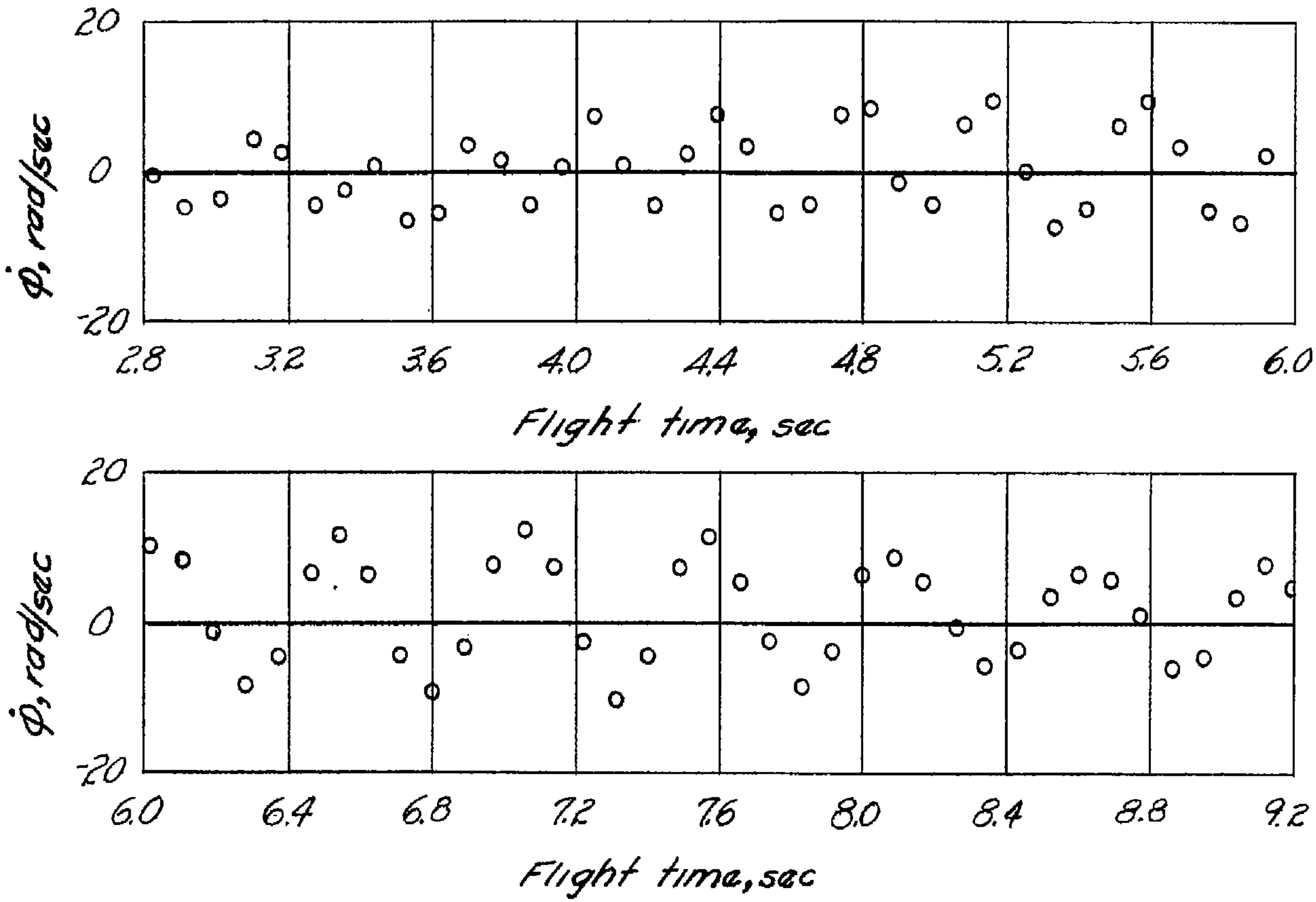

Figure 6.- Rolling velocities as indicated by special radio equipment.

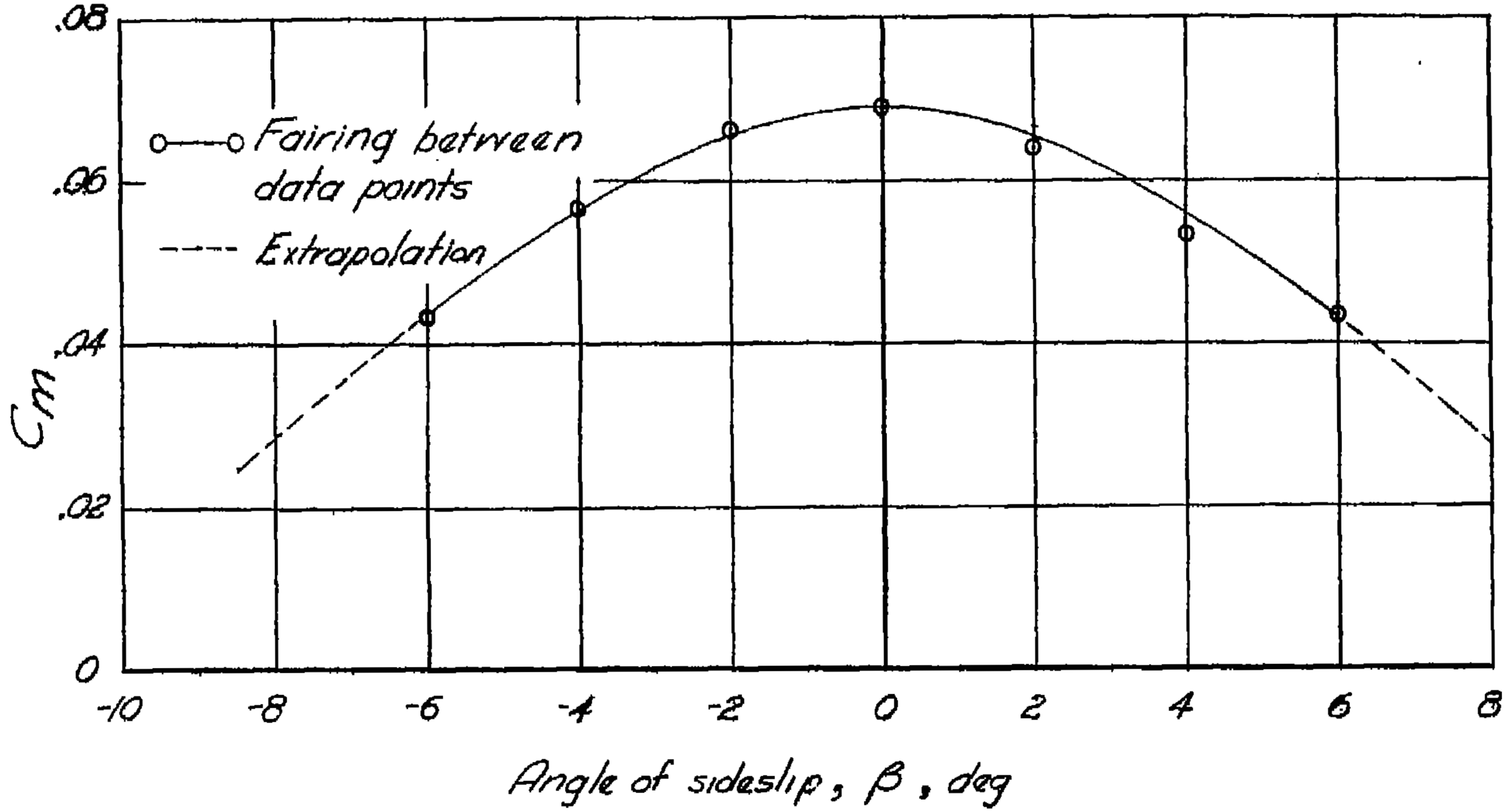

Figure 7.- Static variation of pitching-moment coefficient with angle of sideslip from wind-tunnel tests. $M = 0.17$; $C_{L_{trim}} = 0.36$; $\alpha = 4.25^{\circ}$; $i_t = -1.42^{\circ}$.

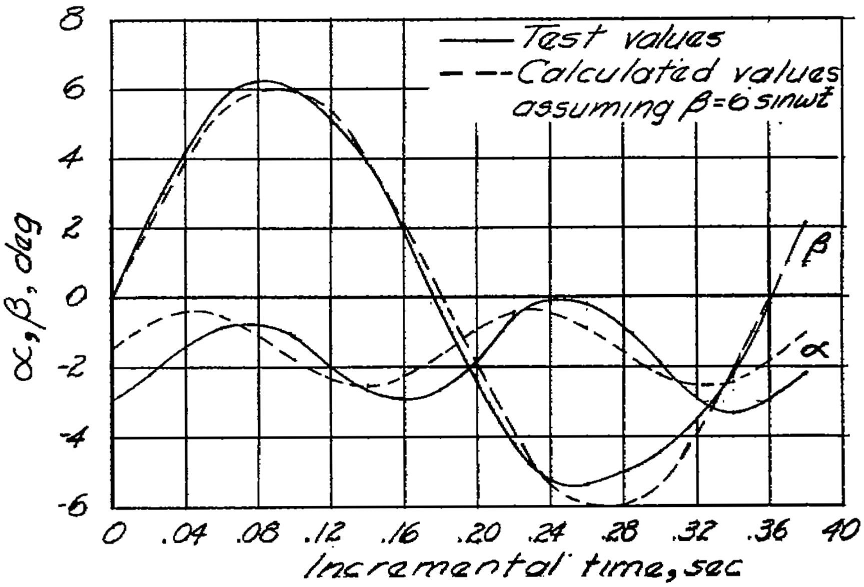

(a) Flight time near 4.2 seconds.

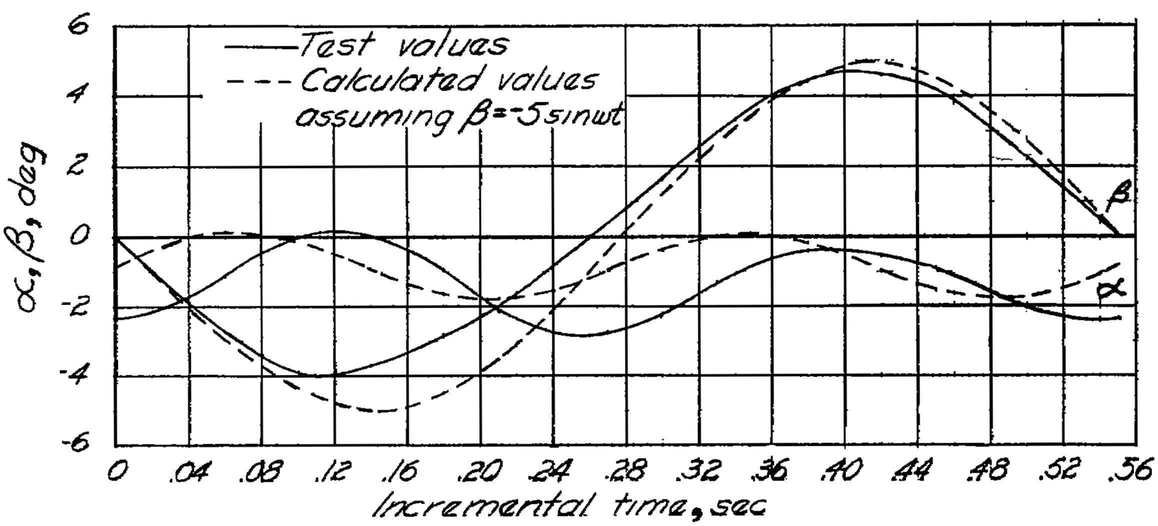

(b) Flight time near 10.2 seconds.

Figure 8.- Comparisons of actual and computed dynamic responses in angle-of-attack to angle-of-sideslip variations.

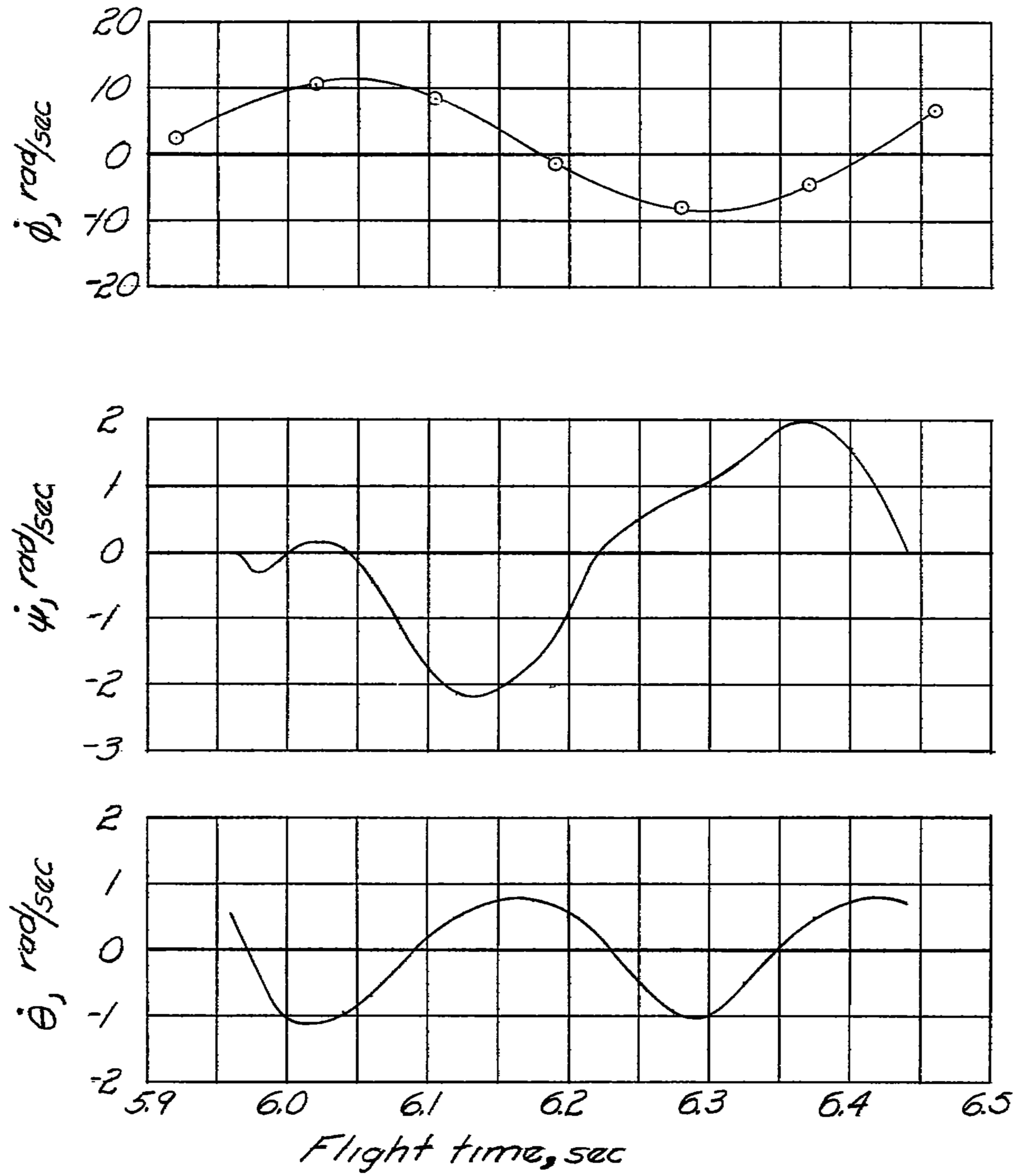

Figure 9.- Rotational velocities at a representative flight time.

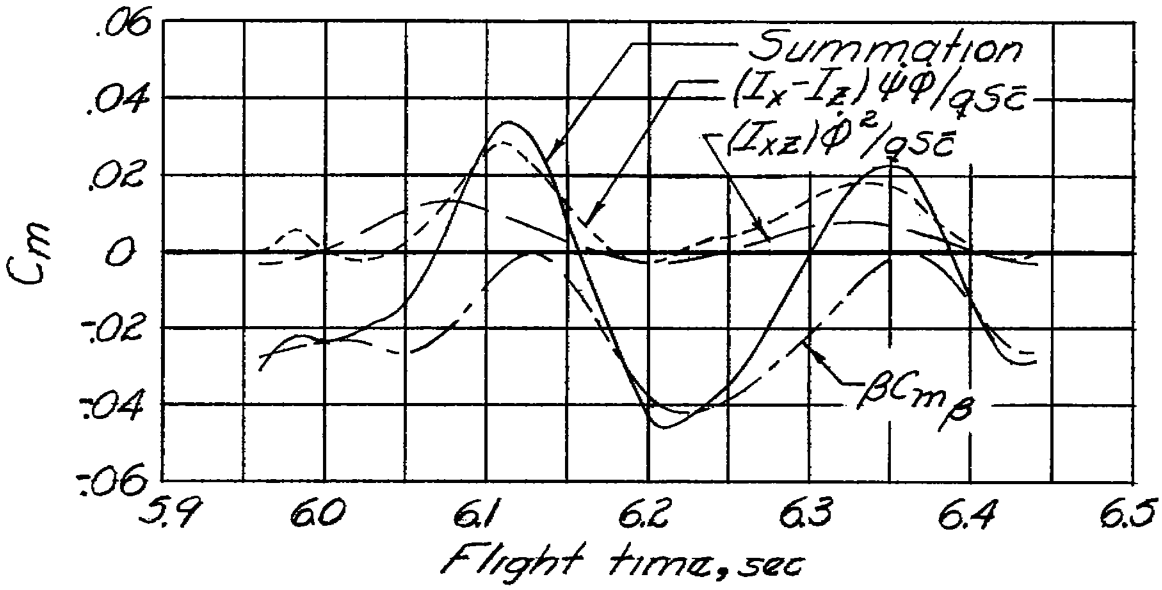

(a) Pitching moments.

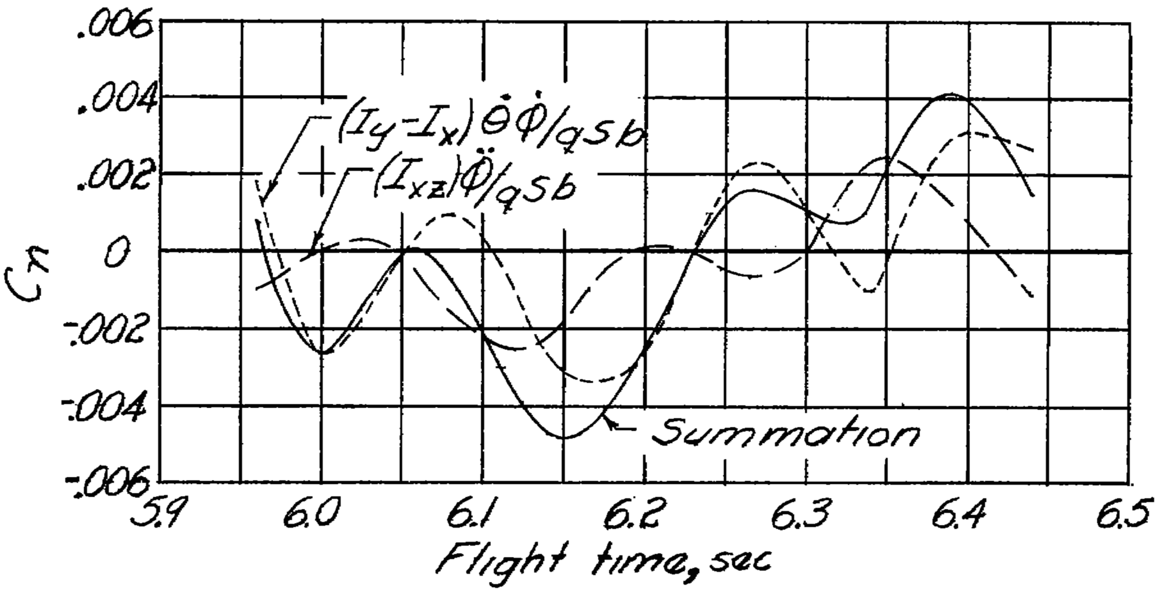

(b) Yawing moments.

Figure 10.- Inertial cross-coupling moments at a representative flight time.

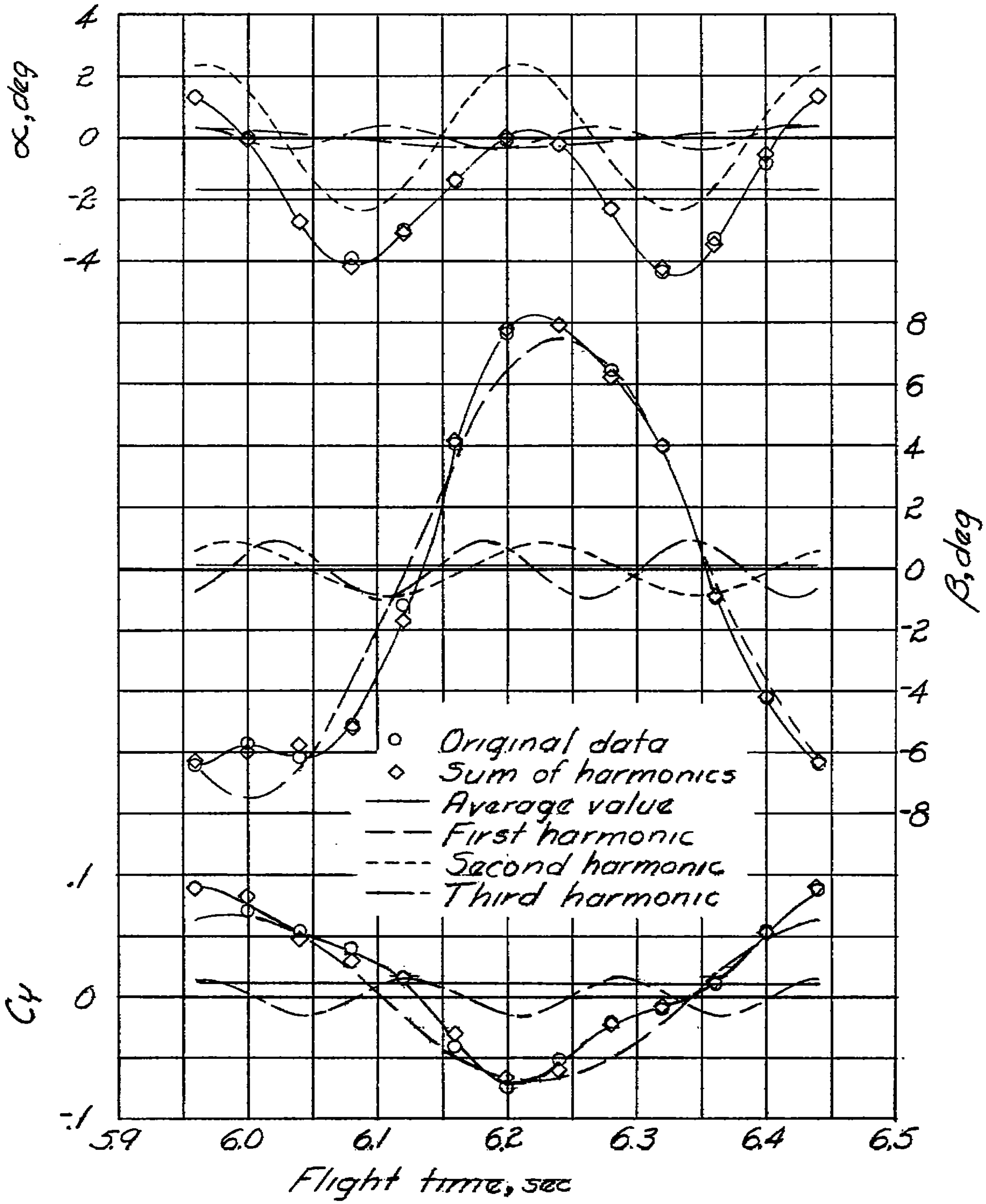

Figure 11.- Harmonic analyses of typical data.

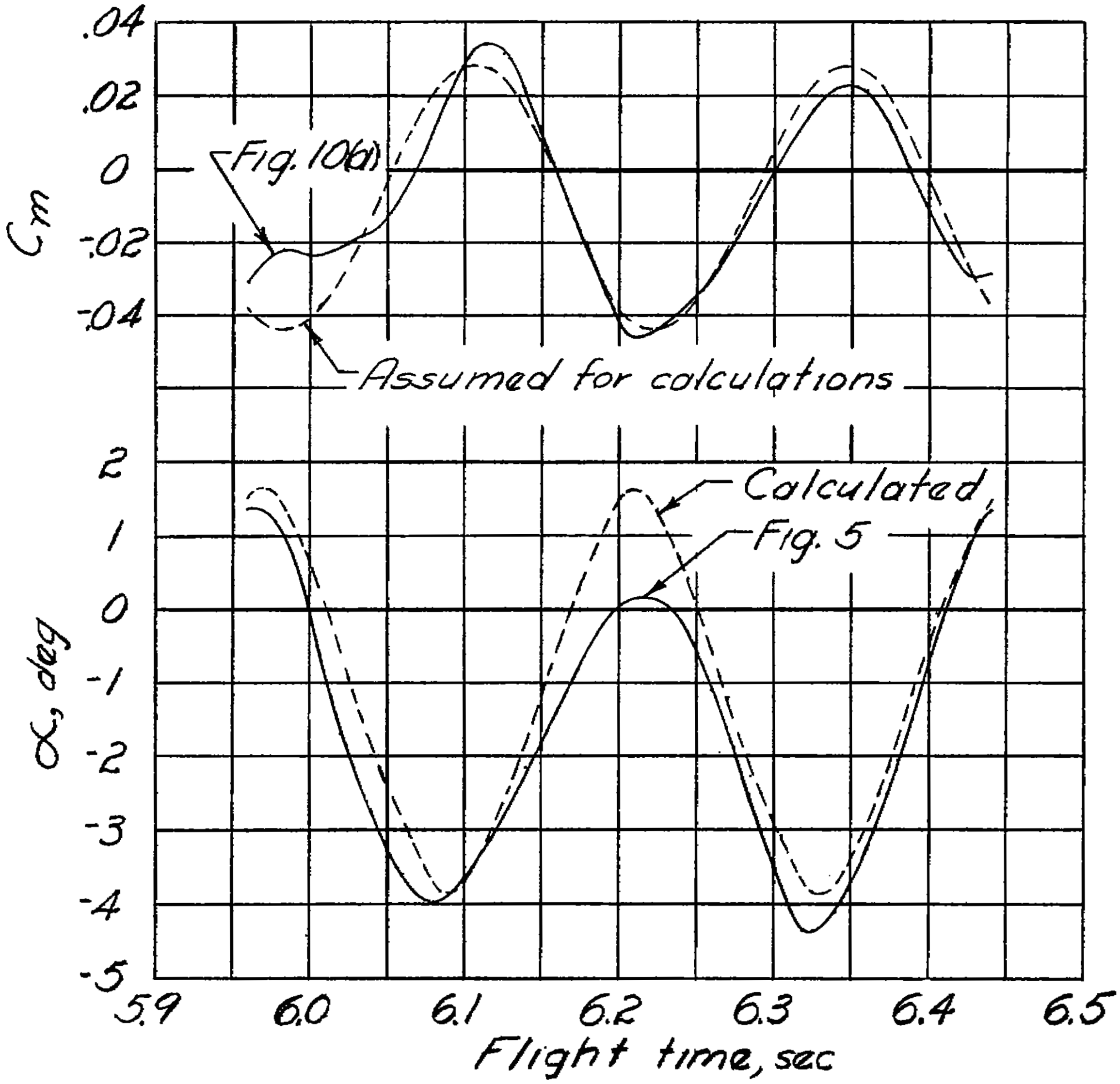

Figure 12.- Comparison of computed and actual angle-of-attack responses to total cross-coupling moments.

NACA-Langley - 5-26-54 - 350

[redacted]

[redacted]